The following publication H. Chen, Y. Du, M. Yuan and Q. H. Liu, "Analysis of the Grounding for the Substation Under Very Fast Transient Using Improved Lossy Thin-Wire Model for FDTD," in IEEE Transactions on Electromagnetic Compatibility, vol. 60, no. 6, pp. 1833-1841, Dec. 2018 is available at https://doi.org/10.1109/TEMC.2018.2807123.

Analysis of the Grounding for the Substation Very Fast Transient Using Improved Lossy Thin-Wire Model for FDTD

Hongcai Chen, *Student Member, IEEE,* Yaping Du, Mengqing Yuan, and Qing Huo Liu, *Fellow, IEEE*

***Abstract*—A thin wire model of conductors with arbitrary cross sections for finite-difference time-domain (FDTD) method is proposed for the study of lightning transients in electrical systems. The proposed thin wire model considers both the frequency-dependent characteristics of the wires and the influences of the surrounding media. The model represents a wire using four FDTD cells with an equivalent side length and modified material parameters. A rational equivalent circuit is added at the center edge of the FDTD cells to represent the internal impedance of the wire. An analytical formula for determining the equivalent side length and the modified material parameters of the FDTD cells are also presented. The proposed formula gives a new prospect to build the thin wire model in FDTD. In this model, the equivalent side length can be set arbitrarily and much larger than the original wire. That can greatly reduce the computation time. Meanwhile, the method can be extended to the thin wire structure with arbitrary cross sections. The model is verified with various measurements. Finally, a practical grounding grid of a substation with external water supply is analyzed.**

Index Terms*—*FDTD*; *substation*; *skin effect*; *lighting*; *grounding grid

I. Introduction

Thin wires, usually representing transmission wires and steel frames, are commonly used in telecommunication systems, electrical power systems and grounding grids. In order to simulate the very fast surge in these wire systems, a full wave solution of Maxwell's equations must be employed where the finite-difference time-domain (FDTD) [1-3] method, method of moments (MoM) [4-6], finite element (FEM) method [7-9], and the discontinuous Galerkin time-domain (DGTD) method [10-12] are widely used. Among these methods, FDTD and MoM are two common methods for calculating lightning transients. MoM is more advantageous to accurately represent the thin wire, while the FDTD is more preferred to handle wires in imperfectly conducting media such as inhomogeneous media and earth soil. However, modeling thin wires is always time consuming in the FDTD because small cross sections of the wires lead to a huge amount of FDTD cells. Meanwhile, common wires with circular cross sections make the meshing with regular rectangular FDTD cells less accurate. On the other hand, an imperfectly conducting medium is required to be accurately modeled to represent currents in the earth. Furthermore, the imperfectly conducting material properties of the wires are also needed for accurate modeling but is seldom addressed in the literature.

There are basically three different models for constructing thin wires for the FDTD. The first is proposed by Holland *et al.* [13], where current and voltage on the wire are described by modified telegraphers equations. The second model is developed by Umashankar *et al.* [14], which is based on the contour-path integral formulation of the FDTD. This model is later improved by adding better treatment of edge effects [15]. However, the major drawback of these two models is that they need to be directly included into the FDTD stencil, making it hard to generalize the model to arbitrarily located wires.

The third model is implemented by equivalently modifying the permittivity and permeability of the FDTD cells surrounding the wire [16]. Noda *et al.* gave an analytical formula to determine the parameters of the thin wire model in the air. Baba *et al.* [17] extended this model to a lossy ground. This approach has advantages of simplicity and robustness and can be directly integrated into any traditional FDTD solvers. However, the analytical formula in Noda and Baba's work is based on the numerical tests, and the coefficients in the formula may vary in different cases. Furthermore, as the skin effect greatly influences the impedance of the wires, the lossless assumption for their models also limits the application of the model.

We propose a new model to accurately represent the thin wire in the FDTD. The proposed method combines the internal/external field concept and the rational equivalent circuit. Both frequency-dependent characteristics and lossy surrounding material are considered. The paper is structured as follows. In Section II, the thin wire model developed by Noda and Baba is briefly revisited. The new thin wire model is demonstrated in Section III. Section IV provides a comparison of results obtained by experiments, previous work and the new model. In Section V, the proposed model is used to analyze the grounding grid of a substation with an external water supply.

II. Thin Wire Model

This section gives a brief review of the thin wire representation developed using modified media. The thin wire is defined as a conductive wire with the cross section smaller than the dimension of a cell. The thin wire is represented by modifying the conductivity, relative permittivity and permeability of the adjacent cells in the FDTD. The equivalent radius of the thin wire, on the assumption of a lossless material, is determined by setting the electric field along the axis of a thin wire to be zero in an orthogonal and uniform-spacing Cartesian grid. An equivalent radius of a thin wire, where the surrounding cell size is Δs, is given by [16]

$$r_0 = 0.23\Delta s \tag{1}$$

The above theory is based on that the fields are quasi-static in the vicinity of the wire. In order to represent the desired radius r_s, medium parameters of the adjacent cells are multiplied or divided by a correction factor m, which is obtained from the transmission line equation as

$$m = \frac{\ln\left(\Delta s / r_0\right)}{\ln\left(\Delta s / r_s\right)} \tag{2}$$

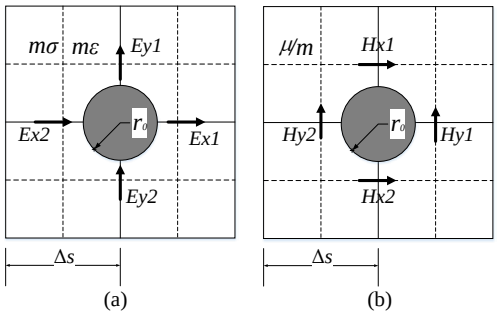

Fig. 1. Thin wire and configuration of adjacent electric and magnetic fields [17]. (a) Four radial electric-field elements closest to the thin wire. (b) Four magnetic-field elements surrounding and closest to the thin wire.

As shown in Fig. 1, the modified conductivity $m\sigma$ and permittivity $m\varepsilon$ of Fig. 1(a) give the same resistance and

capacitance value respectively as that with radius r_s and with original conductivity σ and permittivity ε. In the same manner, the modified permeability μ/m of Fig. 1(b) gives the same inductance value as that with desired radius r_s and with original permeability μ.

III. Proposed Thin Wire Model

A thin wire can be separated into two parts: the internal and external components. The internal component of a wire is associated with the fields inside the wire, while, the external component is determined by the fields from the surface of the wire to the space. This separation is reasonable and convenient to form a thin wire model. The formulation is obvious if we write Maxwell's equations in the vector potential form with the scalar Green's function, as [18]

$$\begin{aligned} \boldsymbol{E} &= \frac{\boldsymbol{J}}{\sigma} + j\omega\boldsymbol{A} + \nabla\Phi \\ \boldsymbol{J} &= \int_0^{r_s} g(\boldsymbol{r},\boldsymbol{r}')\,d\boldsymbol{r}' \\ \boldsymbol{A} &= \frac{\mu}{4\pi}\int_0^{\infty} g(\boldsymbol{r},\boldsymbol{r}')\,d\boldsymbol{r}' = \int_0^{r_s} g(\boldsymbol{r},\boldsymbol{r}')\,d\boldsymbol{r}' + \int_{r_s}^{\infty} g(\boldsymbol{r},\boldsymbol{r}')\,d\boldsymbol{r}' \\ \Phi &= \frac{1}{4\pi\varepsilon}\int_{r_s}^{\infty} g(\boldsymbol{r},\boldsymbol{r}')\,d\boldsymbol{r}' \end{aligned} \tag{3}$$

where $g(\boldsymbol{r},\boldsymbol{r}')$ is the scalar Green's function, $\boldsymbol{r}$ and $\boldsymbol{r}'$ are the source and field points respectively; σ and μ are the conductivity and permeability of the wire respectively; $\varepsilon=\varepsilon'+\sigma'/j\omega$ is the complex permittivity of the surrounding media and σ' is the conductivity of the surrounding media. $\boldsymbol{J}$ is integrated within the wire because the current only flows within the wire. $\boldsymbol{A}$ is obtained by integrating the whole space due to its existence in both inside and outside the conductor. The integrating range for Φ is from r_s to ∞ because charges accumulate at the surface of a conductive wire, namely, electric fields within a wire are zero.

The vector and scalar potentials in (3) can be equivalent as circuit elements. Consequently, a wire is composed of internal impedance indicating the fields within the wire (resistance and inductance), and external impedance (inductance and capacitance) representing the fields outside the wire. As shown in Fig. 2, the internal part is modeled using an equivalent circuit located at the center edge of the cells which is connected to the surface of the cells using a PEC line. The external component is modeled by modifying the parameters of the media in the adjacent four cells surrounding the thin wire similar to the work of Noda *et al* [16]. Hence, it is possible to represent a thin wire using the proposed model in FDTD. Δs can be arbitrarily set and much larger than the dimension of the wires, thus avoiding consuming too much computational resources.

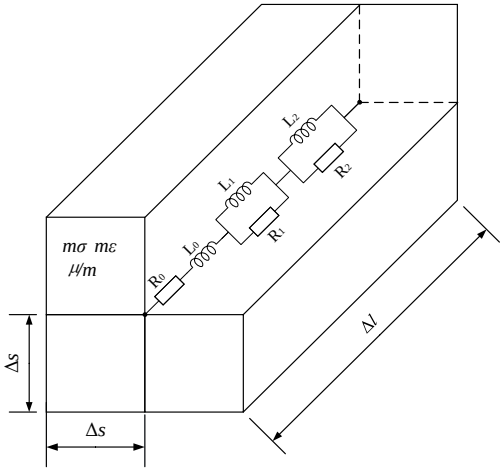

Fig. 2. Proposed thin wire model in FDTD. Equivalent circuit in the center edge of the FDTD cells represents the internal impedance. Four surrounding cells with modified parameters represents external terms.

A. Internal Component

The internal component of a wire is frequency dependent because of the unbalanced field distribution within the cross section of the wire, namely the skin effect. The internal impedance of the wire is frequency-dependent and can be computed numerically or analytically. In case of a wire with circular cross section, the self-impedance Z_{in} is calculated with the explicit formulas [19], as follows:

$$Z_{in} = \frac{j\omega l}{2\pi R_{r_s}} \frac{I_0(R_{r_s})}{I_1(R_{r_s})} \tag{4}$$

where $R_{rs}=(1+j)\cdot r_s/\delta$, δ is the shin depth, r_s and l are the radius and length of the conductor, I_k is the modified Bessel function of order k.

A Vector Fitting (VF) method [20] then is adopted to generate the rational approximation of frequency-dependent parameters. Assume that the impedance in the frequencies of interest is available. Z_{in} can be approximated with rational functions in the form of pole-residue terms as follows:

$$Z_{in}(s) = R_0 + sL_0 + \sum_{m=1}^{N} \frac{s}{s - p_m} R_m \tag{5}$$

where terms R_0 and L_0 are constant, and R_m and p_m are the mth residue and pole which are extracted by the VF method. (5) can be transformed into an equivalent circuit [21] as shown Fig. 3. The extended equivalent network is then added to the FDTD cells. A two-order rational function can accurately approximate the frequency-dependent behavior of the internal impedance.

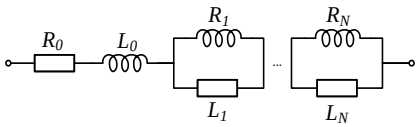

Fig. 3. Circuit represetation of the rational function.

B. External Component

In previous work [16, 22], an expression based on 2D approximation is employed to derive the correction factor m in (2). The intrinsic radius r_0 is approximated as a constant based

on the circular coaxial line formulation. The value of r_0 is decided through the numerical tests.

We employ the external inductance to abstract the correction faction. The linkage fields of the wires are not affected by wire material but the dimensions of the wire and the characteristics of the surrounding media. They are frequency independent. The external inductance of the round wire can be expressed analytically [18] as

$$L_{cir} = \frac{\mu_0 l}{4\pi}\left[\ln\left(\frac{l}{r_s}+\sqrt{1+\frac{l^2}{r_s^2}}\right)-\sqrt{1+\frac{r_s^2}{l^2}}+\frac{r_s}{l}\right] \quad (6)$$

In our model, the thin wire is replaced by a cubic bar with two cells in length as illustrated in Fig. 2. The external inductance of a cubic bar can also be obtained analytically by the total inductance [23] minus the DC internal inductance [24] as

$$L_{rec} = \frac{\mu_0 l}{2\pi}\left(\ln\frac{l}{2\Delta s}+0.5+0.447\frac{2\Delta s}{l}\right)-48\times10^{-9}\cdot l \quad (7)$$

Then, the following relation for correction factor m is obtained by

$$m = \frac{L_{rec}}{L_{cir}} \quad (8)$$

Finally, the conductivity, permittivity and permeability are modified using the correction factor defined in (8). Expression (8) is analytical thus fast in the calculation.

The proposed method can also extend to the wires with an arbitrary cross section. The external inductance of a conductor is determined by the associated magnetic vector potential outside the conductor. It can be therefore calculated using the concept of surface current on the conductor. Thus, external inductance of the conductor can be calculated with the formulas of sheets carrying surface current only as described in [25, 26]. The outer surface can be approximated with a set of planes or sheets which run either in parallel or perpendicularly. The external inductance of such a conductor can then be expressed by using self- and mutual inductance of these sheets using formulations in Appendix. Finally, by substituting the L_{cir} in (8) with the new external inductance, the correction factor is obtained.

IV. Validation

The model described in this paper has been verified by the comparisons with different experimental tests. Firstly, experiments of the rectangle loop composed by flat and round steel are demonstrated to show the performance of our model when material properties and frequency dependent effects are involved. Then, the behavior of the electrode is presented to verify our model in lossy media. In the calculation, to obtain the potential rises of the grounding grid, a grounded reference wire is used. It is vertically located between the wire and the bottom boundary. This reference wire is with an extremely large resistance of 1 MΩ. Therefore, the voltage measured on this wire equals to the potential rises.

In the validation, the traditional FDTD method is also employed for the comparison. The mesh size of the wire must be less than its skin effect depth when using the traditional FDTD method. As shown in Fig. 4 is the cross section of a wire with the radius of 5 mm. The wire is divided into 22 cells to capture the skin effect. Extremely large memory space and extremely long calculation time would be required. While, for thin wire model, the cross section of the wire is only divided into 2 cells.

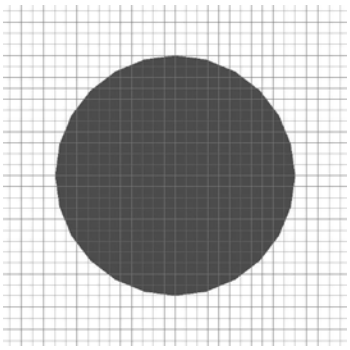

Fig. 4. Circuit represetation of the rational function.

A. Steel Loop Experiment

Steels are commonly used in grounded structures, such as building, tower and grid. These steel wires [27] can be treated as linear magnetic materials with relatively permeability of 35-40 under lightning strikes. They behave a more obvious frequency dependent characteristic than the non-magnetic wires. Therefore, the lossless assumption in the previous thin wire models cannot work well in such cases.

We conducted an experiment where square steel loop was constructed and connected to an impulse current generator as shown in Fig. 5. The current flowing through the loop and the voltage between two ends of the loop were recorded. The material and dimensions of the steels are listed in Table I. DC resistance of the steel loop was measured using a micro-ohmmeter prior to the test.

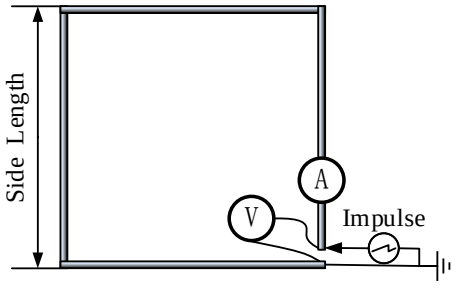

Fig. 5. Experimental configuration of the steel loop. The impulse is injected between two ends of the steel loop. Voltage and current are measured between both ends and at one end of the steel loop, respectively.

TABLE I
MATERIAL AND GEOMETRIC INFORMATION OF STEELS

Steel Shape	Rdc (mΩ/m)	Relative Permeability	W/R (mm)	T (mm)	Length (m)
Rectangle	1.28	40	40	4	1.65
Round	3.16	35	5	-	1

Measured currents were imported into FDTD as current sources. The calculation was performed using conventional FDTD with dense discretization and the thin wire model presented in this paper. Computed voltages of the proposed method match well with the experiment and conventional FDTD for both rectangle and round steel loops as shown in Fig.

6. The calculation shows some oscillation in the voltage curves because the measured current is always accompanied by noise.

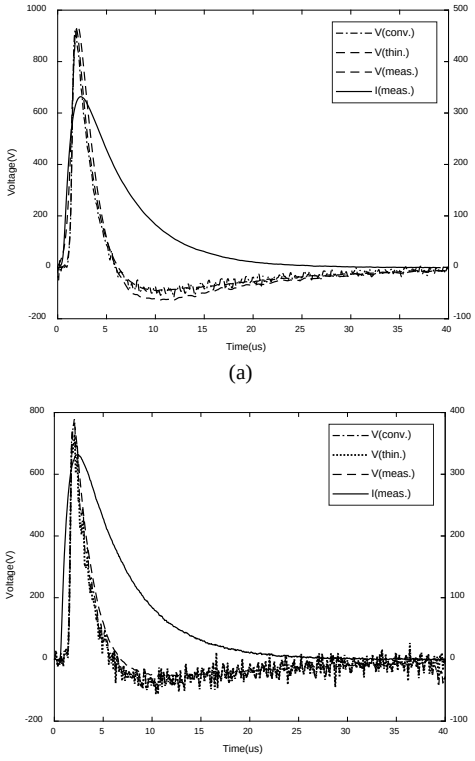

Fig. 6 Comparison of calculated voltages using different model. (a) Rectangle steel loop. (b) Round steel loop. (check the legend is correct or not)

B. Electrode Experiment

Grounding electrodes are built to dissipate the fault currents effectively into the soil. They are buried in the earth and can be modeled using thin wires in a lossy medium. The ground impedance, namely the external term of the thin wire, is dominant [28] in this situation. The internal impedance is negligible.

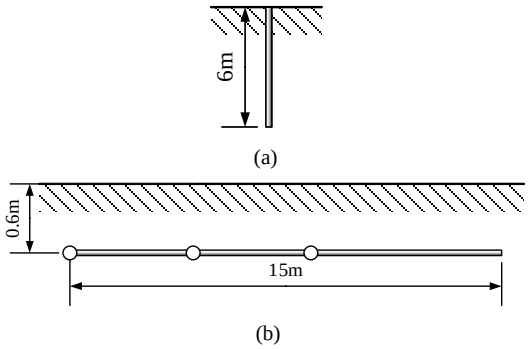

Fig. 7. Experimental configuration of the electrodes. (a) Vertical electrode. (b) Horizontal electrode.

A vertical rod and a horizontal wire tested under a transient impulse excitation by Electricite de France (EDF) [29] are used to verify the model as shown in Fig. 7. Fast impulse currents with front times less than 0.5 us were injected at one end of the electrodes. The parameters of the electrodes and the soil are listed in Table II.

TABLE II
INFORMATION OF ELECTRODES AND THE SOIL

	Material	Radius (mm)	Length (m)	Depth (m)	ρ_g (Ω/m)	ε_g
Vertical	steel	10	6	-	1	8
Horizontal	copper	6	15	0.6	80	15

In the calculation, measured currents were imported into FDTD as current sources. The transient voltages at the injection point of the electrodes were measured. The calculation was performed using conventional FDTD where the cross section of the electrode was meshed densely and the thin wire model proposed in this paper. Results obtained using the conventional FDTD is regarded as the reference. Computed voltages of the proposed method match well with the reference for both vertical and horizontal electrode as shown in Fig. 8. Some differences between calculated and measured results are observed. This is because 8 the measured voltages were amplified by some remaining inductive voltage drop during the wave front along the divider [30]; secondly, the measured currents were imported to the FDTD solver directly which will case numerical oscillation in the calculation.

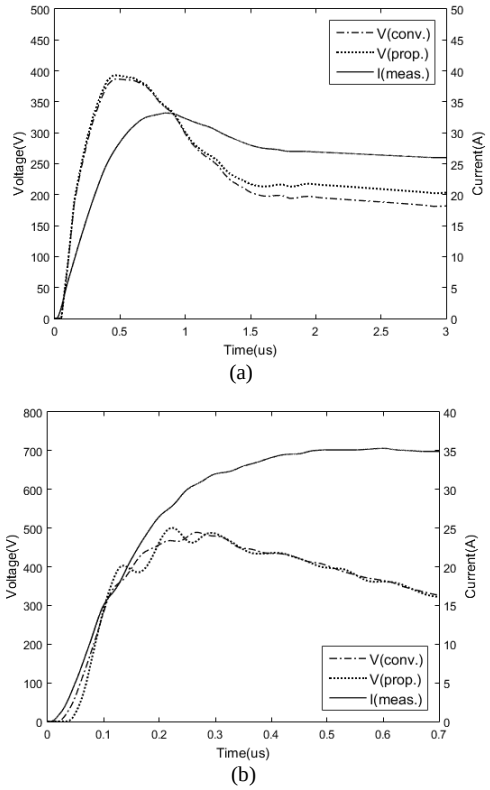

Fig. 8. Comparison of calculated voltages using different model. (a) Vertical electrode. (b) Horizontal electrode.

V. CASE STUDY

In China, substations are sometimes constructed in the areas of high soil resistivity and shortage of groundwater resources. External water supply is constructed to transport the water from

a distanced area. The water pumping station (add pumping for all water stations) is connected to the substation through 1) a low voltage cable that transmits electricity from the substation to the water station, and 2) a metal pipeline that transports the water from the water station to the substation. These two connections will cause the low potential introduction and high potential extraction problems that threat the whole system. Thus, it is necessary to reduce potential differences between the grounding system of the substation and of water station. In this section, the FDTD with the proposed thin wire model is employed to analyze the grounding potential distribution in the grounding system of a substation with external water supply.

The grid configuration [31] is shown in Fig. 9. The main grounding grid is constructed by 50 mm × 5 mm flat steels, with meshes of l0 m × 10 m. A square grid of 4 m × 4 m is built for the water station which is also composed by 50 mm × 5 mm flat steels. Both grounding grids are buried 1 m deep. Two grids are connected by a 50 m pipeline which can be made by metal or PVC. In the simulation, lightning hits on the top left corner of the main grid.

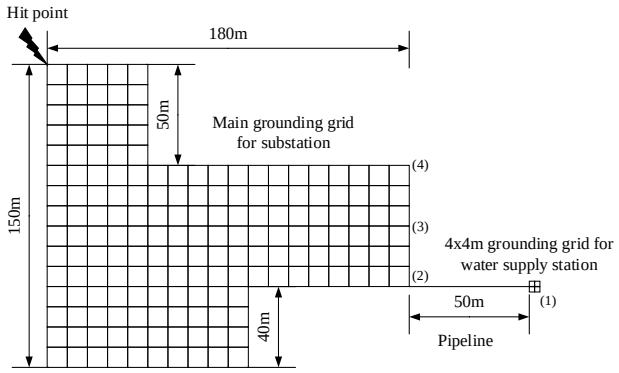

Fig. 9. Grounding system of the substation with external water supply

As the only connection between two grids, pipeline will influence the potential distribution directly. To reduce the step voltages near the water supply station, PVC pipeline is commonly used to disconnect the grid of the water supply from the main grid. In this section, the influence of the PVC configurations on the potential distribution of the whole systems is studied. Four cases are calculated, namely, (a) 50 m metal pipeline, (b) 10 m PVC pipeline near the water station with the remaining 40 m metal pipeline, (c) 10 m PVC pipeline near the main grid with metal pipeline for the left, (d) 50m PVC pipeline.

In the simulation, metal pipeline is modeled as a thin wire, while the PVC pipeline is simply replaced by the soil due to the resistivity of the water being close to the soil and greatly larger than the metal pipeline. The earth is modeled as a three-layer structure whose conductivity and permittivity are described in Table III.

TABLE III
STRUCTURE OF THE SOIL

Layer	Resistivity(Ω/m)	Permittivity	Thickness(m)
1	100	10	1
2	2200	10	500
3	500	15	Infinity

A fast 0.25/100 μs lightning current waveform specified in IEC Standard 62305 [32] is used. The current model is expressed by Heidler's equation[33] as

$$i(t)=\frac{i_{\max}}{\eta}\frac{(t/T)^n}{1+(t/T)^n}\exp(-t/\tau) \tag{9}$$

where we used the following values of Heidler's function parameters: i_{max}=50 kA, T=0.454 μs, τ=143 μs, η=0.993, n=10. The computational domain of 230 m × 320 m × 70 m is surrounded by the Mur's absorbing boundary condition [34]. The plane of the bottom boundary is set as zero potential at -50 m. A non-uniform meshing scheme is employed, and the whole FDTD domain is divided into 340 × 425 × 45 Yee cells. Potential distribution at t=15 μs where the potentials reach peak is displayed in Fig. 10.

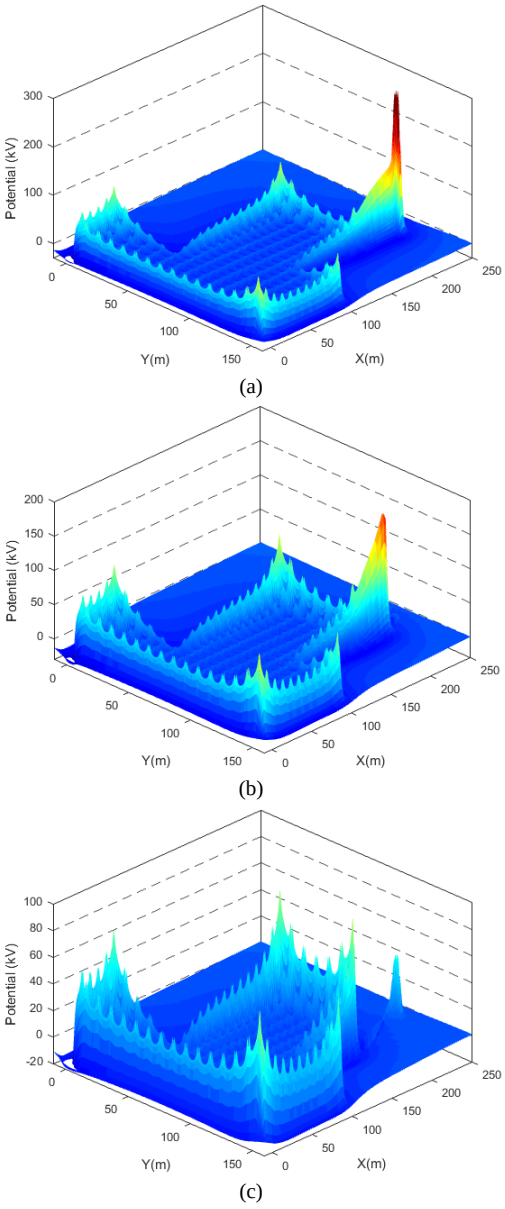

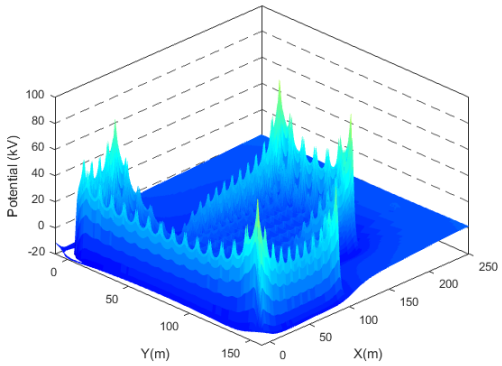

(d)

Fig. 10. Potential distribution of the system at t=15 μs. (a) Total metal pipeline. (b) 10 m PVC pipeline near the water station. (c) 10 m PVC pipeline near the main grid. (d) Total PVC pipeline.

As shown in the Fig. 10, the potential distribution tends to crowd at the edges and corners of the grids. If the pipeline connects with the main grid, the potential rises at (a) the water station and (b) the end of the pipeline are quite large that leads to huge step voltages near the water station. In contrast, if the pipeline has no electrical connection with the main grid, the lightning potential cannot propagate to the water station directly. Thus, the potential rises at the water station become relatively low as displayed in (c) and (d). The optimal solution is using the entire 50 m PVC pipeline for water transport (how low is safe?)

As the water station is fed by the substation though an overhead line, the potential difference between the main grid and the water station is another main concern. A large potential difference will damage the power system in the water station. Choosing a suitable connection point of the overhead line at the main grid may decrease the potential difference. Thus, we select 3 points for evaluation, that is, corner (2), center (3) and far corner (4) as marked in Fig. 9, the potential difference between the connecting point of the main grid and the center of the grid (1) for the water station is measured. (the OHL is open at the pumping station?, what is lightning voltage the isolation transformer is subject to? The discussion is not clear)

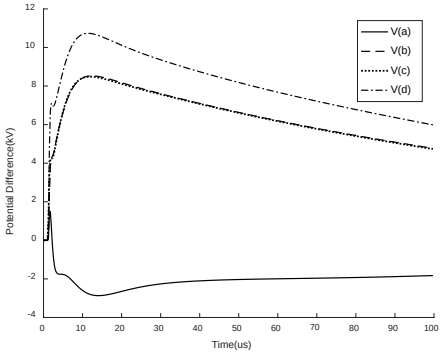

(a)

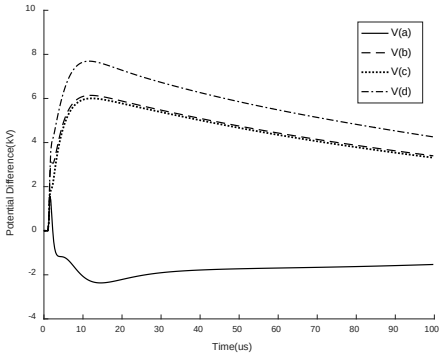

(b)

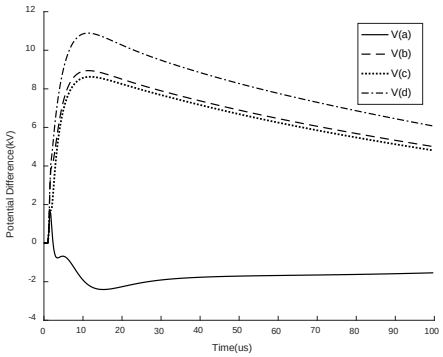

(c)

Fig. 11. Comparisons of voltage differences between point (a) near corner, (b) center, (c) far corner and center of the grid under different configurations.

As displayed in Fig. 11, the potential difference V(a) is the lowest (around 2.5 kV in peak) if the metal pipeline is used. The connection point has little effect on the potential difference between two grids in this configuration. However, since the step voltage is the most critical concern, we prefer to use the configuration (d) in practical construction. In this circumstance, an isolation transformer must be installed to protect the equipment from the high potential damage. Comparison among V(d) with different connection points reveals that the location of the connection point greatly influences the potential difference if two grids are electrically separated. The voltage difference is the lowest if the connection point is at the center of main grid. Its peak value (7.7 kV) is much smaller than that with the connection at the corners, namely, 11.7 kV and 12 kV at near and far corner respectively.

VI. Conclusion

This paper proposed a new thin wire model for the finite-difference time-domain (FDTD) simulation considering both frequency dependent characteristic of the wire and the influence of the surrounding media. The proposed model uses a rational equivalent circuit representing the internal impedance of the wire. The external impedance and the lossy media are modeled by modifying the conductivity, permittivity and permeability around the wire. The experiment shows the proposed model is efficient for modeling thin wires in transient analysis.

The proposed model is applied to analyze the potential distribution in the ground grid of a substation with external water supply. Simulation results show that the step voltages near the water station are very high if the metal pipeline is

employed for water transport. An optimal scheme is using PVC water pipeline as long as possible. An isolation transformer must be installed to protect the facilities in the water station. Meanwhile, the water station is directly supplied by the substation through the overhead line. The location of the connection point of the overhead line at the main grid influences greatly on the potential difference. Leading the overhead line out from the middle of grid gives a much smaller potential difference than that from the corners.

ACKNOWLEDGMENT

The authors would like to thank Wave Computation Technologies Inc. for providing 3D full-wave simulation software. The work leading to this paper is supported by grants from the Research Committee of the HKPolyU (Project No. G-YBN0) and Research Grants Council of the HKSAR (Project No. 152044/14E).

APPENDIX

To obtain the external inductance of wires, the cross sections of wires are discretized only on the surface. As shown in Fig. A1, the cross section of a wire with an arbitrary shape is discretized into line segments (black lines).

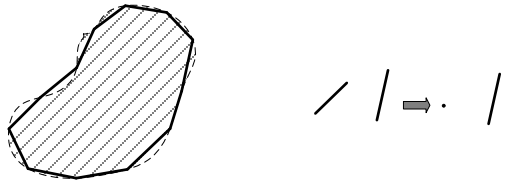

(a) (b)

Fig. A1. Segment scheme of a wire with an arbitray cross section. (a) Cross section of a wire with an arbitrary shape. (b) tape-tape integration is approximated using tape-filament integration.

These segments can be regarded as tapes in 3D coordinates. Taking advantages of the point match concept, a tape-filament scheme is applied for the inductance calculation. Therefore, the field segment is a tape and the source tape is approximated as a filament. Then self and mutual inductance of all segments can be calculated using tape-filament integration.

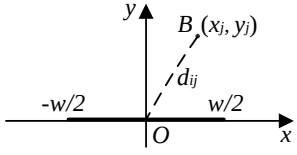

Fig. A2. Geometric information of tape-filament integration in cross section view.

In order to obtain the closed formula of tape-filament integration, a local coordinate system is adopted, as displayed in Fig. A2. Regard the source cell as a point *B*, we have

$$F_{ij} = \frac{2}{S_i l_j}\int_x\int_y \left[l \ln \frac{l+\sqrt{l^2+R_{ij}^{\ 2}}}{R_{ij}} - \sqrt{l^2+R_{ij}^{\ 2}} + R_{ij} \right] dxdy \quad (10)$$

where $R_{ij} = \sqrt{(x_i - x_j)^2 + y_j^2}$. Substitute R_{ij} with d_{ij} in (10) as $l \gg R$. Then the mutual term is becomes

$$F_{ij} = \frac{1}{S_i l_j}\left[f_{ij}(\frac{w}{2}) - f_{ij}(-\frac{w}{2}) \right] \quad (11)$$

where

$$\begin{aligned} f_{ij}(x) = \Big\{ & \left[l \ln(l+\sqrt{l^2+d_{ij}^{\ 2}}) - \sqrt{l^2+d_{ij}^{\ 2}} \right] x \\ & -2ly_j \arctan\frac{x-x_j}{y_j} + 2lx \\ & -l(x-x_j)\ln[(x-x_j)^2 + y_j^{\ 2}] \\ & +(x-x_j)\sqrt{(x-x_j)^2+y_j^2} + y_j^2 \ln[(x-x_j)^2 + y_j^{\ 2}] \Big\} \end{aligned} \quad (12)$$

Thus, the external inductance of the wire is obtained by its circuit connection as

$$L_{ext} = \frac{\mu_0}{4\pi}\sum_{i=0}^{N}\sum_{j=0}^{N}\left(F^{-1}\right)_{ij} \quad (13)$$

REFERENCES

[1] G. X. Fan and Q. H. Liu, "An FDTD algorithm with perfectly matched layers for general dispersive media," *IEEE Transactions on Antennas and Propagation*, vol. 48, no. 5, pp. 637-646, 2000.

[2] Q. Liu, "An FDTD algorithm with perfectly matched layers for conductive media," *Microwave and Optical Technology Letters*, vol. 14, no. 2, pp. 134-137, 1997.

[3] K. Yee, "Numerical solution of initial boundary value problems involving maxwell's equations in isotropic media," *IEEE Transactions on Antennas and Propagation*, vol. 14, no. 3, pp. 302-307, 1966.

[4] R. F. Harrington, *Time-harmonic electromagnetic fields*. Wiley-IEEE Press, 2001.

[5] L. Grcev and F. Dawalibi, "An Electromagnetic Model for Transients in Grounding Systems," *IEEE Transactions on Power Delivery*, vol. 5, no. 4, pp. 1773-1779, Oct 1990.

[6] A. Shoory, R. Moini, S. H. H. Sadeghi, and V. A. Rakov, "Analysis of Lightning-Radiated Electromagnetic Fields in the Vicinity of Lossy Ground," *IEEE Transactions on Electromagnetic Compatibility*, vol. 47, no. 1, pp. 131-145, 2005.

[7] M. Akbari *et al.*, "Evaluation of Lightning Electromagnetic Fields and Their Induced Voltages on Overhead Lines Considering the Frequency Dependence of Soil Electrical Parameters," *IEEE Transactions on Electromagnetic Compatibility*, vol. 55, no. 6, pp. 1210-1219, 2013.

[8] M. Akbari, K. Sheshyekani, and M. R. Alemi, "The Effect of Frequency Dependence of Soil Electrical Parameters on the Lightning Performance of Grounding Systems," *IEEE Transactions on Electromagnetic Compatibility*, vol. 55, no. 4, pp. 739-746, 2013.

[9] J.-M. Jin, *The finite element method in electromagnetics*. John Wiley & Sons, 2015.

[10] L. Fezoui, S. Lanteri, S. Lohrengel, and S. Piperno, "Convergence and stability of a discontinuous Galerkin time-domain method for the 3D heterogeneous Maxwell equations on unstructured meshes," *ESAIM: Mathematical Modelling and Numerical Analysis*, vol. 39, no. 6, pp. 1149-1176, 2005.

[11] Q. Zhan, Q. Sun, Q. Ren, Y. Fang, H. Wang, and Q. H. Liu, "A discontinuous Galerkin method for simulating the effects of arbitrary discrete fractures on elastic wave propagation," *Geophysical Journal International*, 2017.

[12] Q. Zhan, Q. Ren, Q. Sun, H. Chen, and Q. H. Liu, "Isotropic Riemann Solver for a Nonconformal Discontinuous Galerkin Pseudospectral Time-Domain Algorithm," *IEEE Transactions on Geoscience and Remote Sensing*, vol. 55, no. 3, pp. 1254-1261, 2017.

[13] R. Holland, L. Simpson, and K. S. Kunz, "Finite-Difference Analysis of EMP Coupling to Lossy Dielectric Structures," *IEEE Transactions on Electromagnetic Compatibility*, vol. EMC-22, no. 3, pp. 203-209, 1980.

[14] K. Umashankar, A. Taflove, and B. Beker, "Calculation and experimental validation of induced currents on coupled wires in an

arbitrary shaped cavity," *IEEE Transactions on Antennas and Propagation*, vol. 35, no. 11, pp. 1248-1257, 1987.
[15] R. M. Makinen, J. S. Juntunen, and M. A. Kivikoski, "An improved thin-wire model for FDTD," *IEEE Transactions on Microwave Theory and Techniques*, vol. 50, no. 5, pp. 1245-1255, 2002.
[16] T. Noda and S. Yokoyama, "Thin wire representation in finite difference time domain surge simulation," *IEEE Transactions on Power Delivery*, vol. 17, no. 3, pp. 840-847, 2002.
[17] Y. Baba, N. Nagaoka, and A. Ametani, "Modeling of thin wires in a lossy medium for FDTD simulations," *IEEE Transactions on Electromagnetic Compatibility*, vol. 47, no. 1, pp. 54-60, 2005.
[18] C. R. Paul, *Inductance: Loop and Partial*. Wiley, 2011.
[19] S. A. Schelkunoff, "The Electromagnetic Theory of Coaxial Transmission Lines and Cylindrical Shields," *Bell System Technical Journal*, vol. 13, no. 4, pp. 532-579, 1934.
[20] B. Gustavsen and A. Semlyen, "Rational approximation of frequency domain responses by vector fitting," *IEEE Transactions on Power Delivery*, vol. 14, no. 3, pp. 1052-1061, Jul 1999.
[21] K. M. Coperich, J. Morsey, V. I. Okhmatovski, A. C. Cangellaris, and D. E. Ruehli, "Systematic development of transmission-line models for interconnects with frequency-dependent losses," *IEEE Transactions on Microwave Theory and Techniques*, vol. 49, no. 10, pp. 1677-1685, Oct 2001.
[22] Y. P. Du, B. Li, and M. Chen, "The Extended Thin Wire Model of Lossy Round Wire Structures for FDTD Simulations," *IEEE Transactions on Power Delivery*, vol. PP, no. 99, pp. 1-1, 2017.
[23] F. W. Grover, *Inductance calculations: working formulas and tables*. Dover, 1946.
[24] G. Antonini, A. Orlandi, and C. R. Paul, "Internal impedance of conductors of rectangular cross section," *IEEE Transactions on Microwave Theory and Techniques*, vol. 47, no. 7, pp. 979-985, Jul 1999.
[25] H. Chen, Y. Du, and M. Chen, "Lightning current among closely-spaced cables," in *2014 International Conference on Lightning Protection (ICLP)*, 2014, pp. 412-417.
[26] H. Chen and Y. Du, "Model of Ferromagnetic Steels for Lightning Transient Analysis," *IET Science, Measurement & Technology*, 2017.
[27] H. Chen and Y. Du, "Equivalent Circuit Model of Structural Steels for Lightning Transient Analysis," *Submitted*, 2017.
[28] E. D. Sunde, *Earth conduction effects in transmission systems*. New York: Dover Publications, 1968.
[29] F. Mentre and L. Grcev, "EMTP-based model for grounding system analysis," *IEEE Transactions on Power Delivery*, vol. 9, no. 4, pp. 1838-1849, 1994.
[30] L. D. Grcev, "Computer analysis of transient voltages in large grounding systems," *IEEE Transactions on Power Delivery*, vol. 11, no. 2, pp. 815-823, Apr 1996.
[31] B. Zhang, R. Q. Fan, J. Zhu, X. M. Huang, and S. Zhong, "Influence of Extracting High Potential Circuit in External Water Supply System of Substation and its Protective Measures Analyses," (in Chinese), *Shaanxi Electric Power*, 2010.
[32] *Protection of Structures Against Lightning: Part I General principles*, vol. IEC 62305-1, 2010.
[33] F. Heidler, J. M. Cvetic, and B. V. Stanic, "Calculation of lightning current parameters," *IEEE Transactions on Power Delivery*, vol. 14, no. 2, pp. 399-404, Apr 1999.
[34] G. Mur, "Absorbing Boundary Conditions for the Finite-Difference Approximation of the Time-Domain Electromagnetic-Field Equations," *IEEE Transactions on Electromagnetic Compatibility*, vol. EMC-23, no. 4, pp. 377-382, 1981.